System Optimization for Dynamic Wireless Charging Electric Vehicles Operating in a Multiple-Route Environment

Illhoe Hwang, *Student Member, IEEE*, Young Jae Jang, *Member, IEEE*, Young Dae Ko, *Member, IEEE*, and Min Seok Lee, *Student Member, IEEE*

***Abstract*— Dynamic wireless charging (DWC) technology, a novel way of supplying vehicles with electric energy, allows the vehicle battery to be recharged remotely while it is moving over power tracks, which are charging infrastructures installed beneath the road. DWC systems mitigate the range limitation of electric vehicles by using power tracks as additional sources of electric energy. This paper proposes a model and algorithm for optimally designing DWC electric vehicle (EV) systems, particularly those operating in multiple-route environments. Multi-route system comprises several single routes that share common road segments, and the vehicles operating on a specific route are equipped with identical batteries. We build a general model to optimally allocate power tracks and determine the vehicle battery size for each route. Then, we apply a particle swarm optimization algorithm to solve the given multi-route DWC-EV system optimization problem. A numerical example is solved to illustrate the characteristics of the multi-route model, and we show that the proposed modeling approach and algorithm are effective, compared with a mixed integer programming-based exact solution approach. We also conduct a sensitivity analysis to examine the solution behavior of the problem.**

***Index Terms*— Dynamic wireless charging, multiple route, electric vehicle, particle swarm optimization, meta-heuristics.**

I. Introduction

IN CONVENTIONAL electric vehicles (EVs), onboard energy-storage systems such as batteries are charged by plugging them into the grid. However, it is widely known that conventional plug-in EVs have several drawbacks. First, the current plug-in charging method prevents an EV from operating while the battery is being charged, as the vehicle has to remain connected to the grid through the cable connection. The unavailable operation of an EV during charging is referred to as *recharging down time* [1]. A considerable amount of recharging down time is needed, even with the fastest charger available. Another critical drawback of the current plug-in EVs is the limited *per-charging distance*, which requires frequent stops to charge the battery. Thus, the long recharging down time and short per-charging distance of current EVs prevents their use in mass transportation. A mass-transit bus must continuously transport passengers, and thus, cannot make frequent stops to charge a battery. One option is to equip such vehicles with batteries large enough to guarantee continuous services. However, this is not fiscally sound because the larger the battery, the longer the re-charging down time, which would require buses to be idle for long periods.

Wireless charging EVs using wireless power transfer (WPT) technology have been introduced to solve the aforementioned problems. There are two main types of wireless charging: *stationary and dynamic* [2]. *Stationary wireless charging* systems, which only transfer energy to the vehicle when it is parked or not moving, were first introduced to remove the connection cable while charging an electric vehicle from the grid. The more advanced version is the *dynamic wireless charging* (DWC) system, which supplies vehicles with power even while they are in motion. In a DWC system, power supply units called *power tracks* are embedded beneath the road, and transfer electric energy remotely when vehicles travel over them.

The *dynamic wireless charging electric vehicles* (DWC-EVs), also referred to as *move-and-charge* or *roadway-powered EVs*, mitigate the high initial cost of the plug-in EV by allowing the battery to be substantially downsized [2].

A smaller battery that can be powered continuously while in motion makes DWC-EVs a viable option for public transit systems. Currently, there are several research institutions and universities developing and commercializing DWE-EV-based public transportation systems. In 2008, researchers at the Korean Advanced Institute of Science and Technology (KAIST) introduced their first DWC-EV system prototype called the On Line Electric Vehicle (OLEV). The first commercial version of a dynamic charging transportation system was the trolley system in Seoul Grand Park. The second such system, developed for the shuttle buses at the KAIST campus, has been operating since 2012 [3]. In 2013, Gumi city, one of the biggest industrial districts in South Korea, deployed two OLEV-based transit buses to serve a route circulating in

Manuscript received August 3, 2016; revised March 9, 2017 and June 21, 2017; accepted July 16, 2017. Date of publication August 16, 2017; date of current version May 29, 2018. This work was supported by the National Research Foundation of Korea funded by the Korean Ministry of Education through the Basic Science Research Program under Grant NRF-2016R1D1A1B03930712. The Associate Editor for this paper was F. Chu. *(Corresponding author: Young Jae Jang.)*

I. Hwang, Y. J. Jang, and M. S. Lee are with the Department of Industrial and Systems Engineering, Korea Advanced Institute of Science and Technology, Daejeon 34141, South Korea (e-mail: yjang@kaist.ac.kr).

Y. D. Ko is with the Department of Hotel and Tourism Management, College of Hospitality and Tourism, Sejong University, Seoul 05006, South Korea.

Color versions of one or more of the figures in this paper are available online at http://ieeexplore.ieee.org.

Digital Object Identifier 10.1109/TITS.2017.2731787

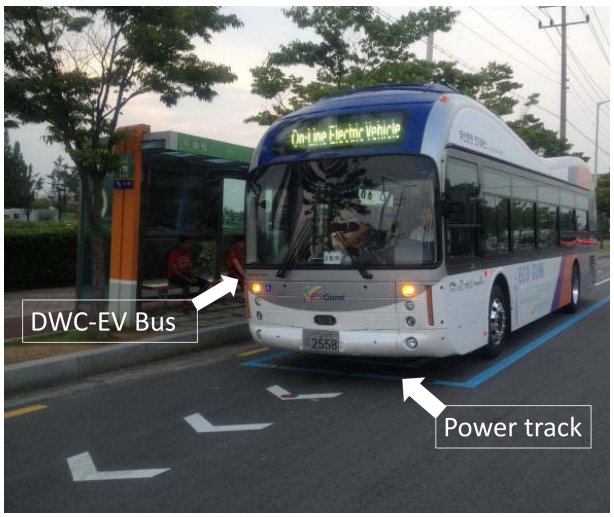

Fig. 1. On line electric vehicle operating in Gumi city.

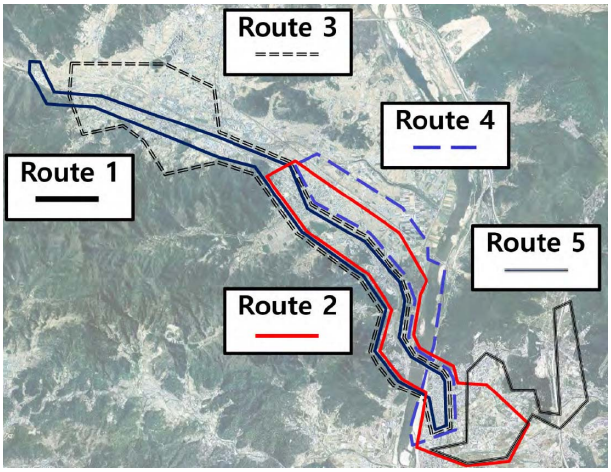

Fig. 2. Public bus transportation lines consisting of multiple routes.

the main part of the city [4]. Fig. 1 shows an OLEV bus in Gumi city being remotely charged by the power track installed beneath the road. These buses are being operated to test the feasibility and stability of the OLEV system in actual traffic conditions.

One of the key questions to answer in the successful commercialization of DWC-EV-based transportation is where to allocate the power tracks for each given route. Because the charging occurs on the power tracks while the vehicle is moving over them, the tracks' locations and lengths directly affect the system's overall performance. This power track location problem is important because the amount of charging depends on the vehicle speed on the tracks, and the number and length of power tracks which are correlated with the battery size. For example, if the battery size is small, more or longer power tracks are needed. Therefore, both the battery size decision and power track allocation should be considered together. Moreover, the costs of the batteries and power tracks account for almost 80% of the total initial investment, which makes these decisions critical in commercializing DWC-EV-based transportation.

Ko and Jang [5] first dealt with the problem of determining the battery size and allocating the power tracks. Their modeling focused on a system with a single fixed route operated by DWC-EVs. As an extension of their research, in this paper we focus on a DWC-EV transportation system that serves multiple routes, as shown in Fig. 2. Some sections of a route are shared with other routes, such that some power tracks can also be shared to reduce installation costs. Specifically, when a road segment overlaps multiple routes, it is beneficial to allocate power tracks on this segment. The optimal positions for power tracks must be decided carefully, and must consider these shared sections of roads to take advantage of multi-route characteristics that saves installation costs. Our extension, which includes multi-route modeling, addresses this issue of shared road segments. The optimal installation cost is further reduced, compared with applying individual single-route optimization to every route. This multi-route problem is motivated by the actual planning of the DWC-EV route design problem for the KAIST OLEV system in Gumi city. As of 2016, the city has extended plans for the OLEV system to serve additional routes. Thus, a multi-route planning methodology is needed for DWC-EV systems.

The major contributions of this paper are as follows. First, it provides a more realistic system modeling method for designing DWC-EV-based public transportation systems by considering multi-route. Second, this paper provides a mathematical model that optimally determines the economical allocation of power tracks, given the battery size. The particle swarm optimization (PSO) method, a powerful meta-heuristic solution procedure presented herein, solves a non-linear optimization problem with continuous variables. Through numerical analyses, we show that the total installation cost of our multi-route modeling approach provides effective charging infrastructure allocation for multi-route cases. Our sensitivity analysis with parameter changes also provides insight into DWC-EV system designs.

The remainder of this paper is organized as follows. Section II summarizes the previous research and current DWC-EV development. Section III describes the general model of a multi-route DWC-EV-based transportation system with detailed design issues. In Section IV, the implementation of the DWC-EV optimization model using a PSO algorithm is presented. In section V, a numerical example is provided to validate the multi-route DWC-EV model. We also evaluate the performance of the PSO algorithm by comparing it with a mixed integer programming model. A sensitivity analysis is also provided for a deeper understanding of the system. In section VI, we summarize the models and approaches and make suggestions for future research.

II. Current Progress on DWC-EV and Related Features

A. Wireless Power Transfer in Electric Vehicles

Wireless charging of EVs using WPT technology has been proposed by several researchers. Bolger et al. [6] first presented the concept in 1978, and it involved transferring electric

energy from a source embedded in the roadway. The inductive charger, a primary coil beneath the roadway, would generate a magnetic field that the pickup device in the vehicle would receive and convert into electric power. More technical details on the developments and efficiency improvements in WPT applied to EVs can be found in [7]–[12].

B. Modern History of the Dynamic Charging Electric Vehicle

In the 1990s, researchers at the University of California Berkeley developed a roadway-powered, 35-passenger electric bus as a proof-of-concept [2]. The complete infrastructure was built for a 213-m-long test track with two 120-m-powered sections. The test results proved the potential of technology, but the findings were limited due to the very low energy transfer efficiency. Around the same time, researchers at Auckland University provided theoretical framework for the dynamic charging solution by proposing a multi-coil track design [2]. The KAIST OLEV uses a resonant coupling technique that supplies 60 Hz of power, which is converted into 20 kHz by the inverter, with a 200 A current flowing through the power track. It has achieved more than 80% charging efficiency with a 170-mm air gap between a pickup device of a vehicle and a power source at road surface. Significant improvements in charging efficiency have led to the development of a commercialized version of OLEV [3]. The technical details of the electro-magnetic coupling and wireless charging are described in [13]–[18].

C. Parameter Design and Charging Infrastructure Allocation for Dynamic Charging EVs

There is a significant body of literature on the charging station allocation problem for pure electric vehicles (PEVs). Ip et al. [19] introduced a model for planning the installation of PEV charging locations in urbanized areas. Using hierarchical clustering analysis, they first constructed demand clusters in urban areas and applied optimization techniques to meet supply and demand. Ge et al. [20] proposed a method for optimizing EV charging station locations using a grid partitioning-based approach. A genetic algorithm was used to solve a given problem by covering traffic flows at each partition. Many other studies have investigated the optimization of charging infrastructures by focusing on the allocation of charging stations [21]–[24]. These approaches have included the location set covering problem, queueing model-based problem, and maximal flow location problem. Grid balance and vehicle-to-grid problems are variations in the classical charging station allocation problems [25]. However, applying approaches developed to solve the conventional PEV charging allocation problem to the DWC-EV problem has limitations. For example, the PEV charging stations must be located in parking lots or other places where vehicles are stationary, whereas the charging infrastructure for the DWC-EV can be installed anywhere on the road. Moreover, the charging time for DWC-EVs is related to the vehicle's speed while driving on the installed charging infrastructure. Therefore, the conventional charging station allocation problem cannot be applied to a DWC-EV system.

Limited research has dealt with the DWC-EV charging infrastructure allocation problem. Pantic et al. [26] designed a heuristic algorithm to optimally allocate the charging infrastructure for DWC-EVs using the standard driving cycle. They conducted a high-level economic analysis of the DWC-EV system by including the charging infrastructure investment cost. Chen et al. [27] provided the mathematical programming model for the charging-lane deployment based on the user equilibrium conditions. They also investigated the economic benefit of charging-lanes against stationary charging facilities [28].

Ko and Jang [5] first introduced the mathematical modeling of charging infrastructure allocation with the battery size decision problem. They analyzed the tradeoff between battery size and charging facility allocation and proposed the particle swarm optimization algorithm to economically determine the battery size and the allocation of the charging infrastructure. Most of the existing research only dealt with single-route cases in which a DWC-EV circulates around a fixed single service route such as the one currently operating on the KAIST campus. To the best of the authors' knowledge, this is the first paper to present the problem of economically determining optimal battery size and charging infrastructure allocation for a multi-route system.

III. Multi-Route DWC-EV

A. Optimization Issue

The optimization issues for DWC-EV-based public transportation systems have been well explained in [5] and other previous studies, including [1] and [29]. The following is a brief review of the general optimization issues, after which the focus shifts to multi-route-specific issues.

The main differences between the multi-route model and single-route cases are as follows:

1) The vehicles servicing different routes may have different battery sizes.
2) A power track, installed beneath road segments shared among different routes, can provide the power to the vehicles operating on the different routes.

We follow the homogeneous battery size assumption made for the single-route case; that is, that the fleet of vehicles operating on the same route has the same battery size. However, in the multi-route model, vehicles operating on different routes may have different battery sizes. Thus, the battery size decision is route-specific. This assumption makes sense, because a route with a relatively short-distance service may not need a large battery. The other main difference is that decisions regarding power track allocation must consider the shared road segments within a multi-route system. It is beneficial to install power tracks under shared road segments.

The optimization problem is qualitatively defined as follows.

Minimize *Total battery cost + Total power track cost*
Subject to: *Every route completes services without running out of energy in the battery*
Decision Variables: *1. Battery size for each route*
2. Power track locations

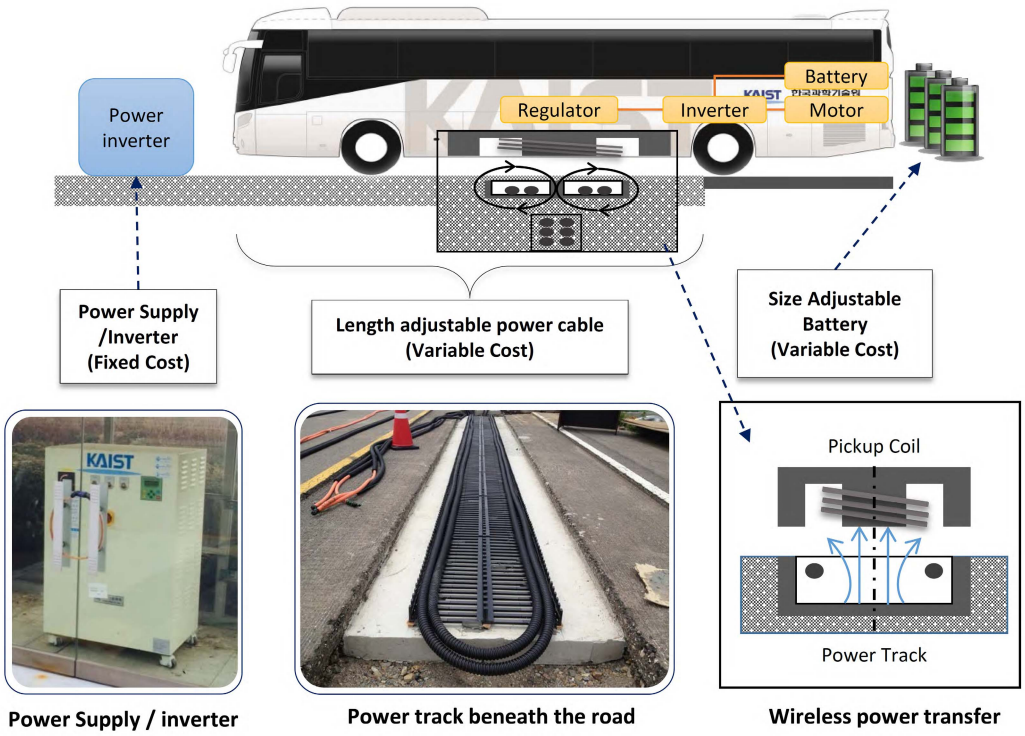

Fig. 3. System components of DWC-EV.

B. System Definition and Assumptions

The DWC-EV system mainly consists of the power track and vehicle units, as indicated in Fig. 3. The vehicle is identical to the normal EV, except it is equipped with a power receiver called a *pickup coil* at the bottom of the vehicle. When the vehicle is driving over the power tracks, it picks up the power and charges the battery. The power track mainly consists of the power supply/inverter unit and power cable, as depicted in Fig. 3. The total cost of the power track is mainly the cost of the power supply/inverter units plus that of the power cable. Given that the cost of the power cable depends on the length of the power track, it is considered as a variable cost of the power track. In contrast, regardless of the length of the power track, one power supply/inverter unit is needed and imposes the fixed installation cost.

The example of multi-route DWC-EV system is described in Fig. 4. The terms and definitions are summarized as follows:

1) Multiple electric vehicles (unless otherwise specified, hereafter the term *vehicle* refers to the wireless charging EV) are operating on each route based on their service schedules.
2) There are multiple stops on each route.
3) Each route is circular and the term *service* represents a single circular trip made by a vehicle.
4) Each route has a start and end point of service called *base station* where vehicles stop for an extended period (20-30 min) between services.
5) Charging always occurs at the base station between services, and a vehicle resumes its next service after fully recharging its battery.

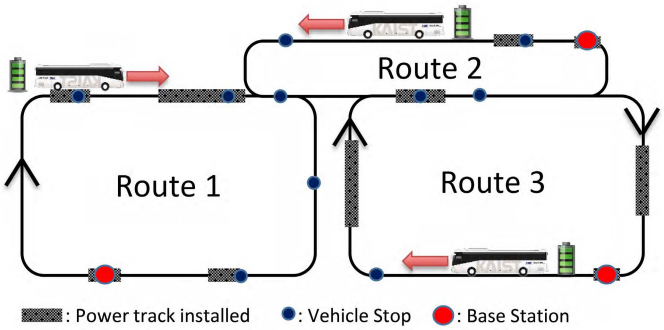

Fig. 4. Example of multi-route configuration.

6) The velocity of a vehicle at any specific point is deterministic and known.
7) Some portions of a route and some stops are shared with multiple routes.
8) Vehicles servicing the same route have the same battery size.
9) The amount of energy required to travel from one place to another can be estimated and known.
10) While a vehicle is operating, there are maximum and minimum allowable energy levels in the battery.

The modeling descriptions for 1 to 6 are the same as in the single-route case. Specifically, the descriptions for 1, 2, 3, and 4 are common settings for public transportation systems. The modeling description for 4 is based on the current operation for the DWC-EVs and other types of EV-based transportation systems. The description for 5 is also based on

the actual operating conditions of commercialized DWC-EV systems [5]. The description for 6 is based on the data collected from the DWC-EV, and the validation is confirmed in [1] and [29]. The descriptions for 7 and 8 are commonly found in public transit bus systems in urban environments.

The modeling description for 9 concerns the energy demand estimation. We define $D(x^s, x^e)$ as the energy requirement to travel from point x^s to x^e. A previous study [5] used the analytical approximation model to estimate this quantity. Another study [1] used the experimental data to estimate it. It is also common that this energy requirement quantity is known and given for charging station allocation problems for conventional EVs [30], [31]. Thus, we also assume that this quantity is known. Readers interested in the method of estimating the energy requirements may refer to [1] and [5].

Note the modeling description for 10. Specifically, E_0^r is the battery capacity of the vehicle operating on route r, and we assume that an allowable range for the battery while driving is between E_{high}^r and E_{low}^r, where

$$E_{high}^r = e^h \times E_0^r, \tag{1}$$

$$E_{low}^r = e^l \times E_0^r, \tag{2}$$

$$0 < e^l < e^h < 1. \tag{3}$$

The constants e^h and e^l are for the upper and lower limits of charging and discharging, respectively. Note that the charging and depleting behavior of a battery is nonlinear, but the amount of charging within a range E_{high}^r and E_{low}^r is assumed to be linearly proportional to the charging time. Here, we define the constant rate of charging as P_{cs}. Then, the amount of charging while the vehicle is on the power track from time t_1 to t_2 is evaluated as:

$$P_{cs} \cdot (t_2 - t_1)\,. \tag{4}$$

This linear charging assumption is based on the previous works and other DWC-EV-related research described in [26], [32], and [33]. With the linear-time charging behavior, the energy level at a specific point in the travel can be estimated from the travel time from a reference point. For instance, suppose that a vehicle is traveling at a specific point, x, according to a reference point such as a base station. Let t be the traveling time from the reference point. Then, the travel point and time have the following relationship.

$$x = \int_0^t V(t)dt, \tag{5}$$

where $V(t)$ is the known velocity of the vehicle at time t. Let us now represent (5) as the function $x = F(t)$. Note that this function is monotonically increasing; therefore, there exists a unique solution for its inverse function, i.e., $t = F^{-1}(x)$. Because $V(t)$ is known, we can calculate the amount of energy charged from one point to another with the equations (4) and (5). For instance, suppose that a power track is installed from x^s to x^e, as shown in Fig. 5. Then, the energy charging amount from x^s to x^e, which is defined as $S(x^s, x^e)$, is

$$\begin{aligned} S(x^s, x^e) &= P_{cs} \cdot (F^{-1}(x^e) - F^{-1}(x^s)) \\ &= P_{cs} \cdot (t^e - t^s). \end{aligned} \tag{6}$$

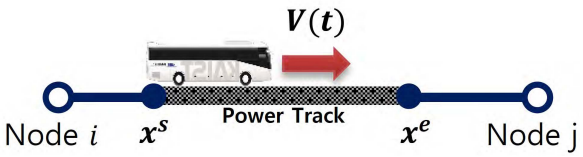

Fig. 5. Vehicle moves from x^s to x^e, and $V(t)$ is known.

The detailed logical relationship between the time and temporal values and the experimental validation of the actual DWC-EV system can be found in [1], [5], and [29]. The time and displacement relationships described in (4) and (5) are significant in our modeling. That is, we can estimate the energy usage and charging amount used from one point to another, as long as the deterministic travel velocity is known.

C. Optimization Model and Algorithm

This section explains the modeling approaches and algorithm for the DWC-EV system. For our convenience, we explain using an illustrative case in Fig. 6, which consists of two separate routes and multiple stations. Some of the stations and segments are shared by different routes. First, we define the following sets to describe the multi-route system:

- **V**: Set of nodes; $\mathbf{V} = \{1, 2, ..., n\}$
- **L**: Set of directed links; $\mathbf{L} = \{(i, j) \mid i, j \in \mathbf{V}, i \neq j\}$
  - if $(i, j) \in \mathbf{L}$, then node i directly followed by j
- **R**: Sequential set of nodes; $\mathbf{R_r}$=$\{R_r(1), R_r(2),..., R_r(k), R_r(k+1)\}$
  - where $(R_r(1), R_r(2))$, $(R_r(2), R_r(3))$,..., $(R_r(k), R_r(k+1)) \in L$
  - $R_r(k+1) = R_r(1)$ ($\because$ Base station assumption)

The set **V** includes all of the nodes in the routes. In our model, stations and *merge/separate points* are defined as nodes. For example, in Fig. 6, nodes 1, 4, 6, and 8 represent stations while nodes 2, 3, 5, and 7 represent merging points. The set **L** includes all of the links connecting the nodes. In our example, there are 10 links, $\mathbf{L} = \{(1,2), (2,7), (3,1), (3,4), (4,2), (5,3), (6,5), (7,6), (7,8), (8,5)\}$. Note that (i, j) is a directed link as the vehicle moves from node i to j. The set $\mathbf{R_r}$ presents the sequence of nodes on route r, which indicates the route index set, and in our example, $r = \{1, 2\}$. We define $R_r(k)$ as the element of the set $\mathbf{R_r}$, indicating the kth node on route r. Note that $\mathbf{R_r}$ is a sequential set where the nodes are arranged in the sequence of the vehicle path. Moreover, due to the circular route assumption, the node in the first element of set $\mathbf{R_r}$ is identical to that in the last element. For instance, in Fig. 6, $\mathbf{R_1} = \{1, 2, 7, 8, 5, 3, 1\}$ and $\mathbf{R_2} = \{6, 5, 3, 4, 2, 7, 6\}$. Note that set $\mathbf{R_r}$ is route-specific while link set **L** and node set **V** are not.

The basic idea of the modeling is that we first decompose the routes into multiple links, as shown in Fig. 7, and determine the power track allocations for each link. Specifically, as shown in the figure, the routes are broken down into 10 different links. Then, the allocation of power tracks is investigated for each link. Note that the link is not route-specific; that is, in Fig. 7, link $(2, 7)$ is part of both routes 1 and 2.

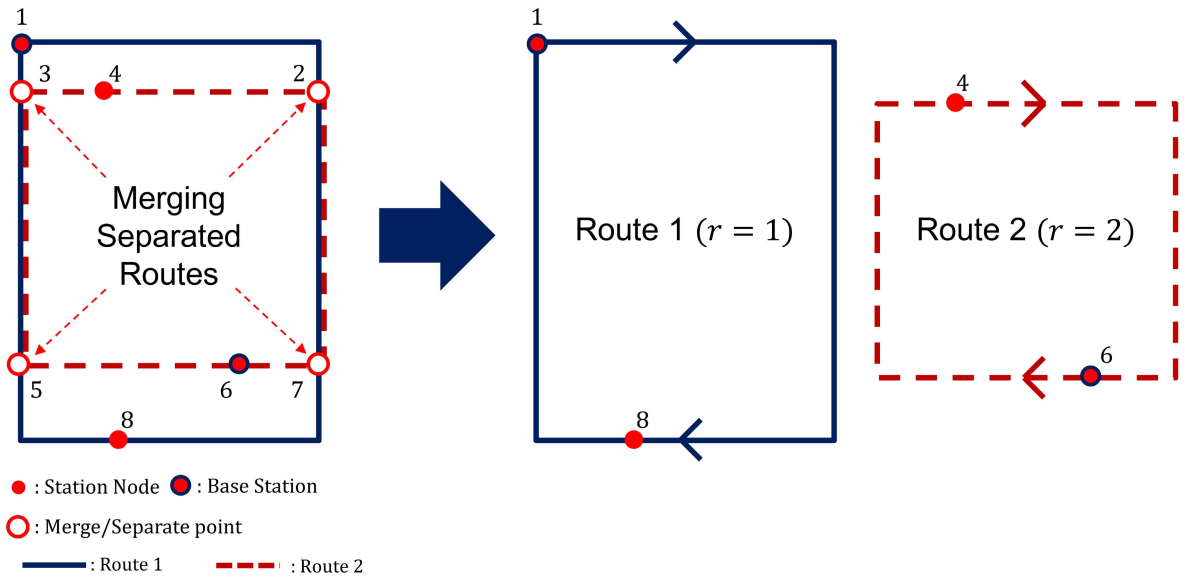

Fig. 6. Multi-route system comprises routes 1 ($r = 1$) and 2 ($r = 2$).

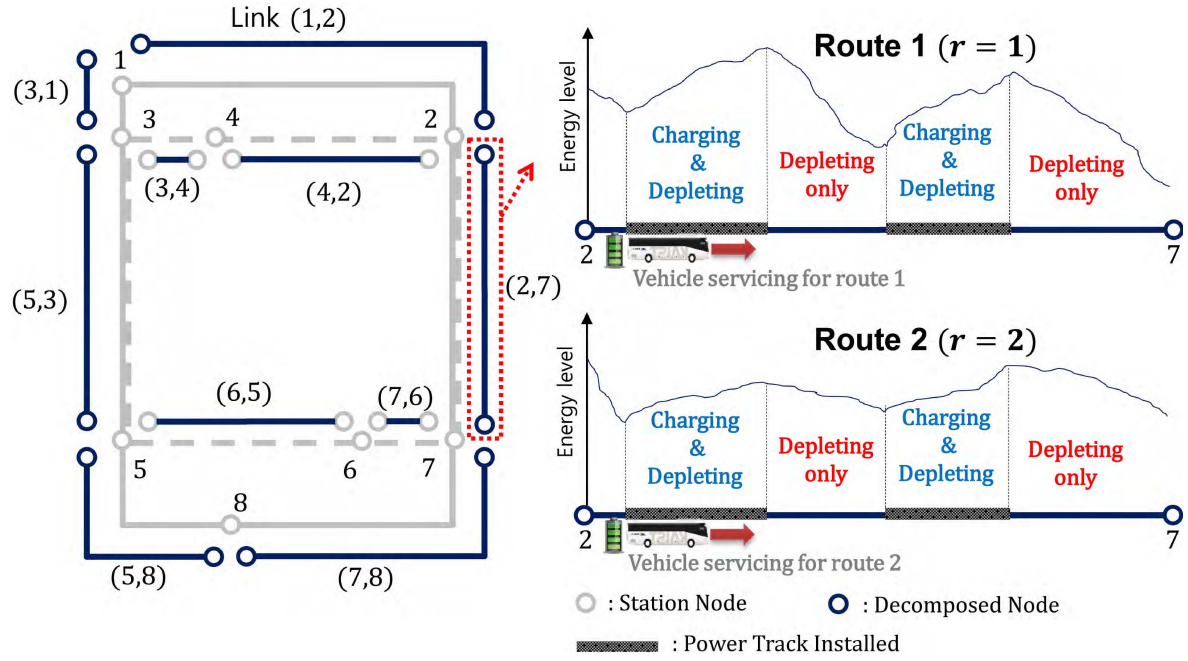

Fig. 7. Entire routes are decomposed into multiple links.

The decomposed links are logically related by conserving the energy level of a vehicle at the edges of the links. We introduce the parameters, which logically connect the decomposed links: $e^r(i, j)$ and $f^r(i, j)$, which are the energy level in the battery, respectively, at the beginning and the end of link (i, j) for route r. Suppose that a vehicle for route 1 is about to leave node 2. Then $f^1(1, 2)$, the energy level in the battery of the vehicle at the end of link $(1, 2)$, is identical to $e^1(2, 3)$, the energy level at the beginning of link $(2, 3)$. Therefore, the decomposed links have the following energy relationship:

$$f^r(i, j) = e^r(j, k), \quad \forall r, \text{ and } \forall\ (i, j),\ (j, k) \in \mathbf{L}. \tag{7}$$

Once the links are decomposed, the power tracks are allocated for each of the decomposed links. As Fig. 7 shows, we define $x^s_{(i,j)}(n)$ and $x^e_{(i,j)}(n)$ as the start and end points of the nth power track allocated in link (i, j), respectively. They are continuous variables that indicate relative distances from the beginning of the link. Note that for each link, we define the maximum number of power tracks as $N_{(i,j)}$ and assume that this number is known and given.

Note that the decision variables are not route-specific. Because a power track is installed on a link, the former can supply energy to any vehicle operating on the latter. The right panel in Fig. 7 illustrates the energy level in the battery of the vehicle running on link $(2, 7)$. In the figure, two power

tracks are allocated to the link, and the energy levels of the vehicle for routes 1 and 2 are depicted. Given the different velocity profile, the energy requirements of the vehicles for routes 1 and 2 are different, even if they are running on the same link. As a result, the power tracks should be allocated to meet the energy requirement of the vehicles on both routes. For example, in Fig. 7, the power tracks on link $(2, 7)$ should be allocated to meet the energy demands of the vehicles running on routes 1 and 2. We define $E^r(x^*_{(i,j)})$ as the energy level at point $x^*_{(i,j)}$, $^* \in \{s, e\}$, for the vehicles running on route r. Therefore, $E^r(x^s_{(i,j)}(n))$ and $E^r(x^e_{(i,j)}(n))$ are the energy levels at which the vehicle is at the entering and leaving points, respectively, of the nth power track on link (i, j). Another decision variable is the battery size, E^r_0, which is represented as the battery level for the vehicle running on route r. Note that this variable is route-specific. Then, we can define the following energy balance equations:

$$E^r(x^e_{(i,j)}(n)) = \min\,[E^r(x^s_{(i,j)}(n)) + S^r(x^s_{(i,j)}(n), x^e_{(i,j)}(n)) - D^r(x^s_{(i,j)}(n), x^e_{(i,j)}(n)), E^r_{high}], \quad \forall r,\ \forall (i,j),\ \forall n, \quad (8)$$

$$E^r(x^s_{(i,j)}(n+1)) = E^r(x^e_{(i,j)}(n)) - D^r(x^e_{(i,j)}(n), x^s_{(i,j)}(n+1)), \quad \forall r,\ \forall (i,j),\ n = |1, \ldots, N_{(i,j)} - 1. \quad (9)$$

First, (8) represents the energy level when a vehicle is about to leave the power track allocated on $x^e_{(i,j)}(n)$. This energy level should be identical to the level when the vehicle enters the power track, $E^r(x^s_{(i,j)}(n))$, plus the energy supplied by $S^r(x^s_{(i,j)}(n), x^e_{(i,j)}(n))$, minus the energy used when it has been driving over area $D^r(x^s_{(i,j)}(n), x^e_{(i,j)}(n))$ while it has been driving over the power track. Because this energy level should not be greater than the battery's upper limit of E^r_{high}, it is in the minimum function.

Likewise, the equation (9) indicates the energy level when the vehicle is about to enter a power track at $x^s_{(i,j)}(n+1)$, where the $(n+1)$th power track is installed. This is estimated as the energy level when the vehicle leaves the previous power track, $E^r(x^e_{(i,j)}(n))$, minus the energy that has been used since the last power track, $D^r(x^e_{(i,j)}(n), x^s_{(i,j)}(n+1))$.

The energy level $E^r(x)$ for every point x has to be within the lower and upper limits of the battery; specifically, E^r_{low} and E^r_{high}, respectively.

$$E^r_{low} \le E^r(x) \le E^r_{high}, \quad \forall r,\ \forall x. \quad (10)$$

The equations (8), (9), and (10) are the primary constraint equations for the optimization problem. In other words, the power tracks must be allocated to meet the energy requirement in (10) while following the energy balance equations in (8) and (9).

Note that these energy balance equations are similar to those for the single-route case, except that they are defined for multi-route. Even if vehicles run over the same links, (i, j), and as long as they are different route vehicles, they have different balance equations. With these equations, the power tracks must be allocated to meet the energy requirements of all of the routes.

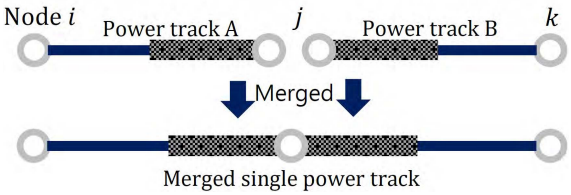

Fig. 8. Two power tracks are combined on the intersection.

TABLE I
DECISION VARIABLES FOR THE MULTI-ROUTE DWC-EV SYSTEM

Decision Variable	Definition
$x^s_{(i,j)}(n)$	Start point of the nth power track on link (i, j)
$x^e_{(i,j)}(n)$	End point of the nth power track on link (i, j)
E^r_0	Battery capacity of the vehicle on route r

TABLE II
NOTATIONS FOR THE MULTI-ROUTE DWC-EV SYSTEM

Notation	Definition
$\mathbf{V}$	Set of nodes in the multi-route
$\mathbf{L}$	Set of links in the multi-route
$\mathbf{R_r}$	Sequential set of nodes indicating route r
r	Route index
$e^r(i,j)$	Energy level in the battery at the beginning of the link (i, j) for route r
$f^r(i,j)$	Energy level in the battery at the end of the link (i, j) for route r
$E^r(x)$	Energy level at a point, x, for the vehicles running on the route r
$S^r(x, x')$	Amount of energy charged when a vehicle on route r is running from x to x'
$D^r(x, x')$	Amount of energy used when a vehicle on route r is running from x to x'
$N_{(i,j)}$	Maximum number of power tracks that can be installed on the link (i, j)
$l_{(i,j)}$	Length of the link (i, j)
k^r	Number of vehicles operating in route r

D. Objective Function

The objective of the optimization is to minimize the total investment, including the total battery and installation costs of the power tracks. The cost evaluation of the power tracks is more complicated for the multi-route than for the single-route case. For instance, as Fig. 8 shows, there are two links: (i, j) and (j, k). Suppose that the algorithm allocates power track A to link (i, j) and power track B to link (j, k). Once the decomposed links are combined, these two power tracks become a single unit. In this case, the fixed cost only needs to be incurred for either A or B, not both. The variable cost of the power track, which is determined by its length, can be individually evaluated for each decomposed link. However,

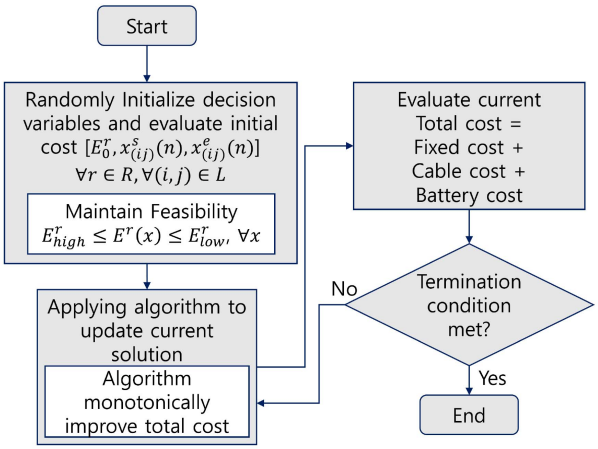

Fig. 9. Solution procedure overview.

the fixed cost is evaluated after the links are combined. We provide an algorithm to determine the fixed cost of the power tracks in the next subsection.

The parameters, decision variables, and other quantities are defined in Tables I and II. The high level algorithm structure of the optimization model is described in Fig. 9

$$\text{Minimize} c_{cable} \sum_{\forall (i,j)\in \mathbf{L}} \sum_{\forall n} (x_{(i,j)}^e(n) - x_{(i,j)}^s(n)) + c_{bat} \sum_{\forall r} k^r \cdot E_0^r + F_{fixed}(\cdot) \quad (11a)$$

$$E^r(x_{(i,j)}^e(n)) = \min [E^r(x_{(i,j)}^s(n)) + S_{(i,j)}^r(x_{(i,j)}^s(n), x_{(i,j)}^e(n)) - D_{(i,j)}^r(x_{(i,j)}^s(n), x_{(i,j)}^e(n)), E_{high}^r], \quad \forall r, \ \forall (i,j), \ \forall n \quad (8)$$

$$E^r(x_{(i,j)}^s(n+1)) = E^r(x_{(i,j)}^e(n)) - D_{(i,j)}^r(x_{(i,j)}^e(n), x_{(i,j)}^s(n+1)), \quad \forall r, \ \forall (i,j), \ n = 1, ..., N_{(i,j)} - 1 \quad (9)$$

$$E^r(x_{(i,j)}^s(1)) = e^r(i,j) - D_{(i,j)}^r(0, x_{(i,j)}^s(1)), \quad \forall r, \ \forall (i,j) \quad (11b)$$

$$f^r(i,j) = E^r(x_{(i,j)}^e(N_{(i,j)})) - D_{(i,j)}^r(x_{(i,j)}^e(N_{i,j}), l(i,j)), \quad \forall r, \ \forall (i,j) \quad (11c)$$

$$f^r(i,j) = e^r(j,k), \quad \forall r, \ \forall (i,j), \ \forall (j,k) \quad (11d)$$

$$S^r(x_{(i,j)}^s(n), x_{(i,j)}^e(n)) = P_{cs}(F^{-1}(x^e) - F^{-1}(x^s)), \forall r, \quad \forall (i,j), \ \forall n \quad (11e)$$

$$E_{low}^r \le E^r(x) \le E_{high}^r, \quad \forall r, \ \forall x \quad (11f)$$

$$x = F(t) = \int_0^t V(t)dt, \quad \forall x \quad (11g)$$

The objective function is (11a). The first term is the variable cost of the power track and the second is the total battery cost in the system. The third term, $F_{fixed}(\cdot)$, is the fixed cost function, which will be discussed in the next subsection. The equations from (11b) to (11f) are the constraints. Specifically, (11b) and (11b) are the energy balance equations, and (11b) and (11c) are the boundary conditions for each link. The constraint (11d) is the energy equations on the merge/separate points. The decomposed links are logically related to these equations. The amount of energy supplied from each allocated power track is evaluated from (11e). Finally, the energy bounds of the battery are expressed in (11g) and (11f).

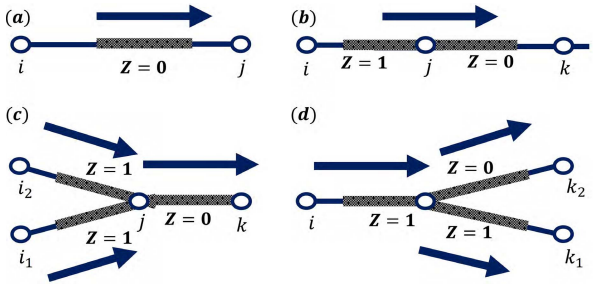

Fig. 10. Summary of counting fixed cost.

E. Fixed Cost Evaluation Algorithm

Fig.10 illustrates the issues and the high-level algorithm of the fixed cost evaluation. Z is the binary indicator, which is 0 if the fixed cost is imposed on the corresponding power track, and 1 otherwise. For example, in Fig.10(a), the power track is located in the middle of the link. In this case, the fixed cost should be imposed on the power track, and therefore, $Z = 0$. In contrast, if a power track is located at the edge of the link, it is not simple. For the case in Fig.10(b), the power track in link (i, j) and the one in (j, k) are connected once the links are combined. The arrow indicates the direction the vehicle is moving. In this case, the two power tracks are connected, and only one unit of fixed cost is imposed on either the first or the second, not both. The proposed fixed cost evaluation algorithm identifies the connectivity of the power tracks and selects an appropriate power tack on which a fixed cost is imposed. The basic idea is as follows. Once the algorithm identifies that more than two power tracks are connected, it always imposes the fixed cost on the last one. For instance, in Fig.10(b) and (c), the power track in link (j, k) is the last one among the connected power tracks, and therefore, $Z = 0$. If more than one power track is connected as depicted in Fig.10(d), then the one with the highest link index, (j, k_2), imposes the fixed cost and $Z = 0$, while the other power track, (j, k_1), does not and $Z = 1$.

To calculate fixed cost, we define a binary variable $Y_{(i,j)}(n)$, which is 1 if the nth power track on link (i, j) exists (if $x_{(i,j)}^e(n) - x_{(i,j)}^s(n) > 0$), and 0 otherwise. Then, the number of fixed costs imposed on entire routes can be specified as follows:

$$\sum_{\forall (i,j)\in L} \sum_{\forall n} \left(Y_{(i,j)}(n) - Z_{(i,j)}(n)\right). \quad (12)$$

Therefore, F_{fixed} in equation (11a) is

$$F_{fixed} = c_{fixed} \cdot \sum_{\forall (i,j) \in L} \sum_{\forall n} \left(Y_{(i,j)}(n) - Z_{(i,j)}(n) \right), \quad (13)$$

where c_{fixed} is a unit fixed cost of the power track.

Note that the power track with $Z = 0$ does not mean that the activities causing the fixed cost, including the installation of power inverters/suppliers, will occur on this particular power track. We only use the value Z to count the number of connected power track groups. Hence, Z is a logical indicator without physical meaning. The details of how the algorithm identifies the connected power tracks and evaluates the Z value for each power track are explained in the Appendix.

IV. Particle Swarm Optimization on DWC-EV Optimization Problem

In this section, we introduce the particle swarm optimization (PSO) algorithm as a solution procedure for the multi-route DWC-EV optimization problem. PSO is a meta-heuristic algorithm derived from bird flocking, and is based on the mechanism of a flock searching with information sharing. Each particle explores the search space based on a combination of personal experience and memory of every point the entire swarm has ever visited. Particles simultaneously share information about sweet spots with each other as a group. The PSO is used as the solution algorithm due to its simplicity. The PSO's simple structure is easily modifiable, and requires less computational memory and fewer lines of code. Moreover, only a few parameters need to be adjusted, which makes it particularly easy to implement. As such, PSO is considered a robust and efficient algorithm for solving nonlinear, non-differentiable, multi-modal problems. PSO also effectively deals with continuous search spaces. Our multi-route formulation contains many decision variables defined in a continuous real-valued domain, and the PSO algorithm is suitable for solving these types of problems. PSO's theoretical and practical characteristics are found in [34]–[38].

A. PSO Algorithm

The purpose of the algorithm is to find an optimal position with the best fitness function value in a given solution space. Individual particle j explores and exploits the space by evaluating its current position vector at time t, $\mathbf{Pos}_j^t$, which is a set of decision variables for a specific problem. $fitness(\mathbf{Pos}_j^t)$ is an objective function value of the problem evaluated on $\mathbf{Pos}_j^t$. The algorithm is successful when the particles are able to reach the problem's optimal solution.

Each particle j has a memory of the *personal best point* ever visited ($\mathbf{Pbest}_j$). Meanwhile, an entire swarm preserves one *global best point* ($\mathbf{Gbest}$). From particle j's current position, $\mathbf{Pos}_j^t$, its next position $\mathbf{Pos}_j^{t+1}$ is determined by combining three velocity vectors: (1) its current velocity vector $\mathbf{Vel}_j^t$, (2) a vector toward its private best $\mathbf{Pbest}_j - \mathbf{Pos}_j^t$, (3) and a vector toward the global best $\mathbf{Gbest} - \mathbf{Pos}_j^t$. Fig. 11 depicts the three vectors determining particle j's next position at time t. In the figure, the position $\mathbf{Pos}_j^{t+1}$ is basically calculated as follows:

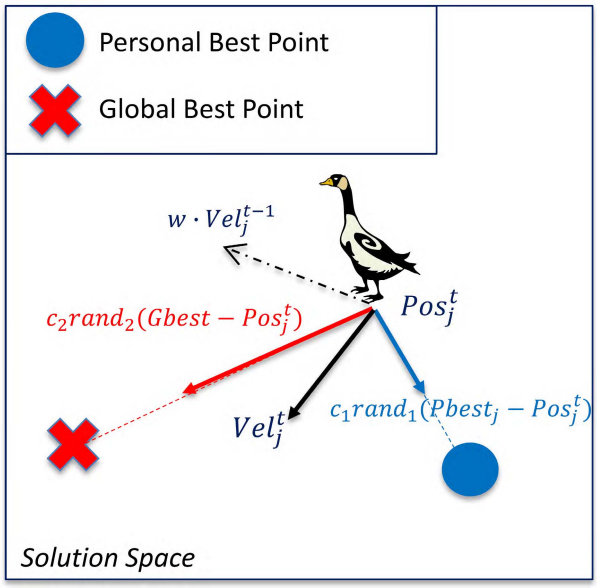

Fig. 11. Three vectors determining the next position of the jth particle.

$$\mathbf{Pos}_j^{t+1} = \mathbf{Pos}_j^t + \mathbf{Vel}_j^t. \quad (14)$$

Then, the velocity vector $\mathbf{Vel}_j^t$ on equation (14) is determined as a linear combination of the three vectors:

$$\mathbf{Vel_j^t} = w \cdot \mathbf{Vel_j^{t-1}} + c_1 \cdot rand_1 \left(\mathbf{Pbest}_j - \mathbf{Pos}_j^t \right) + c_2 \cdot rand_2 \left(\mathbf{Gbest} - \mathbf{Pos}_j^t \right), \quad (15)$$

where c_1 and c_2 are constants, $rand_1$ and $rand_2$ are the uniform random variables that follow $U(0, 1)$, and w is the inertia of the PSO algorithm. Detailed explanations for each parameter can be found in [39].

The standard PSO procedure is as follows:

1) Initialize position and velocity of each particle.
2) Evaluate fitness function value of each particle.
3) Update private best of each particle.
4) Update global best position of entire swarm.
5) Determine next position of each particle using equations (14) and (15).
6) Repeat procedures 2 to 5 until the termination criteria are met.

B. Implementing PSO on the Multi-Route DWC-EV Problem

To solve a problem with PSO, the elements of position vector $\mathbf{Pos}_j^t$ are defined. Then, the decision variable of the DWC-EV problem and the start and end points of power tracks $x_{(i,j)}^s(n)$ and $x_{(i,j)}^e(n)$, and the battery capacity of each route E_0^r, are used as elements of $\mathbf{Pos}_j^t$. Then, $\mathbf{Pos}_j^t$ is defined as follows:

$$\mathbf{Pos}_j^t = [E_0^1, E_0^2, ..., E_0^m, x_{(i,j)}^s(1), ..., x_{(i,j)}^s(N_{(i,j)}), x_{(i,j)}^e(1), ..., x_{(i,j)}^e(N_{(i,j)})], \quad \forall (i,j) \in L. \quad (16)$$

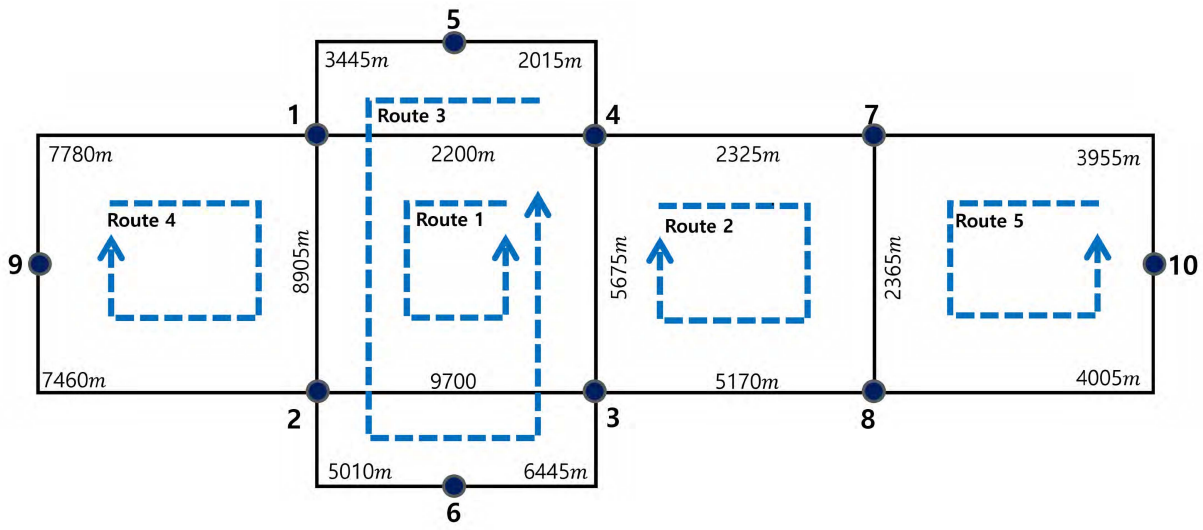

Fig. 12. Each route has a common base station; Route 1: 1-2-3-4-1, Route 2: 3-4-7-8-3, Route 3: 1-2-6-3-4-5-1, Route 4: 1-2-9-1, Route 5: 7-8-10-7.

We use the objective function of the optimization problem to evaluate each particle:

$$\begin{aligned} &\mathit{fitness}(\mathbf{Pos}_j^t) \\ &= c_{bat} \cdot \sum_{\forall r} k^r E_0^r + c_{cable} \cdot \sum_{\forall (i,j)} \sum_{\forall n} \{x^e_{(i,j)}(n) - x^s_{(i,j)}(n)\} \\ &\quad + c_{fixed} \cdot \sum_{\forall (i,j)} \sum_{\forall n} \{Y_{(i,j)}(n) - Z_{(i,j)}(n)\}. \end{aligned} \tag{17}$$

If the decision variables violate the energy balance equations and constraints described in previous sections, we impose a large penalty value on its fitness value.

Because the problem has a large number of decision variables and constraints, a good initial feasible solution can help the algorithm to obtain a good solution. Previous research on the DWC-EV problem revealed that the solution tends to allocate power tracks to cover the points where the speed of a vehicle is low. This strategy guarantees longer charging times with shorter power tracks installed. We regarded this idea as a solution property of the problem. Therefore, we initialized the position of the power tracks to cover all of the points where the speed of the vehicle is below the given threshold. Compared with the random initialization, this method provides good initial feasible solutions and helps the algorithm to quickly converge to the optimal solution.

V. Numerical Analysis

In this section, we validate the model and algorithm with a numerical example. We present a case study to show how the proposed model and algorithm outperformed the existing method of power track allocation. We compared our model to the mixed integer programming (MIP)-based approach to evaluate its performance. Finally, we performed an extensive sensitivity analysis by varying the parameters to show how the system's behavior aligns with our insight.

A. Basic Result

Fig. 12 presents the entire set of routes that we consider for the numerical analysis. The routes and velocity profiles are generated using the geometric data sets of five public transit bus lines in Gumi City. These data are based on the actual placement of bus stops and velocity regulations in the region. A total of 76.5 km of road is divided into multiple shared and non-shared links and contains multiple routes. Table III summarizes the data set used. Fixed deterministic velocity profiles is used for the allocation problem, and this assumption is common in the literature of the charging facility allocation [22], [40], [41]. The system parameters and cost of each component are summarized in Table IV. The number of EVs, k^r, equals 15 on every route, so that in total 75 vehicles are operating.

We use the proposed particle swarm optimization method to obtain the basic numerical results on a given multiple route. These results are summarized in Table V. The optimal allocation of power tracks with respect to their position and length was determined algorithmically. In total, 57 power tracks are needed to supply additional energy to the EVs, with a summed length of 8,715 m. Almost all of the power tracks are located at bus stops, where an EV's velocity drops to zero, because the amount of battery charging is proportional to the time that the EV spends on the power track. The given allocation of power tracks maximizes cost efficiency. The optimal battery sizes for Routes 1 to 5 are 301.89 kWh, 123.21 kWh, 351.77 kWh, 280.09 kWh, and 109.64 kWh, respectively.

B. Result Comparison With Greedy-Approach

We now present the effectiveness of the proposed multiple-route model by comparison with the greedy single-route optimization approach, where the optimal power track allocations and battery size are determined for each route individually. The proposed algorithm is compared with the greedy method to highlight the behavior and characteristics of the solution.

TABLE III
SUMMARY OF EACH ROUTE DATA

Route Summary	Route 1	Route 2	Route 3	Route 4	Route 5
Total length (m)	26,480	15,535	31,495	24,145	10325
The number of stops	30	30	32	23	25
Average Speed (m/s)	15.73	14.27	16.08	16.63	13.53
Total energy requirement (kWh)	218.22	120.17	259.24	192.46	108.03

TABLE IV
SYSTEM PARAMETERS

Component	Value
Number of EVs for a route	15
Battery cost ($/kWh)	400
Fixed cost of power track installation ($/each)	5000
Unit cable cost ($/m)	60

TABLE V
RESULT OF NUMERICAL EXAMPLE

Result	Value
Total investment cost	7795928.11
Optimal battery route 1 (kWh)	301.89
Optimal battery route 2 (kWh)	123.15
Optimal battery route 3 (kWh)	351.37
Optimal battery route 4 (kWh)	280.04
Optimal battery route 5 (kWh)	109.58
Total length of power track (m)	8,578.14
Number of power track installed	57

Again, the goal of this comparison is not to demonstrate that the proposed optimization method is superior to the greedy method. Instead, the comparison will enable us to better understand the solution.

For the purpose of comparison, we obtained the optimal solutions of the greedy method and the proposed multiple-route model with varying numbers of vehicles on the route. We attempted to calculate the cost efficiency of installing power tracks on shared links with increasing numbers of EVs from different routes utilizing the same power tracks. We successively increased the number of vehicles on each route from 5 to 50 in increments of 10 and solved each resulting problem.

The results are compared in Table VI. The multiple-route approach proves to be more cost-effective than the greedy method for every tested scenario. Moreover, the greedy approach always requires a larger optimal battery size than the multiple-route method. Thus, the length of the power track is always smaller in the greedy approach because the EVs have greater battery requirements. As the number of vehicles increases, the multiple-route approach tends to install more power tracks on the road while reducing the battery size.

To understand the solution behavior in detail, we next investigated what fraction of the road part of the shared links is utilized as power track. First, we define the utilization ratio of shared links as follows:

$$\text{Util. of shared links} = \frac{\sum \text{Length of power tracks on shared links}}{\text{Total length of shared links}}$$

In our example, links $(1, 2)$, $(3, 4)$, and $(7, 8)$ are shared links with a combined length of 16.9 km (22% of the total), and the remaining links are non-shared, totaling 59.5 km (78). We measured the utilization of shared links in both the multiple-route and greedy approaches. Fig. 13 shows the results. Figs. 13a and 13b represent the total length of power track installed on shared and non-shared links. Fig. 13a indicates the result from the multiple-route approach and 13b that from the greedy approach. In Fig. 13a, the length of power tracks installed on shared links is always longer than on non-shared links, even though the shared links are only 22% of the entire route. The greedy approach has the opposite tendency, as shown in Fig. 13b. Moreover, Figs. 13c and 13d show the utilization ratio of both approaches. In Fig. 13c, when the number of vehicles reaches 35, almost every road part of the shared links is utilized as a power track. In contrast, the greedy approach utilizes many fewer shared links, as shown in Fig. 13d. The rate of increase of utilization is similar for shared and non-shared links in this figure.

These results indicate that the algorithm of the multiple-route approach actively searches for solutions that reflect the characteristics of the shared links. It explicitly considers the cost efficiency of power tracks installed on shared links. Lengthening the power tracks on the shared links enables more EVs to use the common power tracks. Therefore, the size of the battery in each EV can be reduced. In summary, the proposed approach maximizes the benefit of installing power tracks on shared links, especially when numerous EVs operate on the route

C. Results Comparison With an Exact Algorithm

We now use the MIP-based multi-route case as a benchmark to validate the proposed model and algorithm. Note that due to the nonlinear nature and complexity issue, it was not easy to construct a model and an algorithm capable of generating an exact solution. However, a small-sized, multi-route problem can be constructed as a form of MIP model by discretizing the route into small pieces. As illustrated in Fig. 14, the routes were discretized into small segments (e.g., 1 m long). Then, the energy required to travel each segment was estimated. In this format, the decision is whether a particular segment

TABLE VI
RESULTS COMPARISON: MULTIPLE ROUTE AND GREEDY APPROACH

Number of vehicle	10	20	30	40	50
Total cost: multiple	5.41×10^6	10.10×10^6	14.53×10^6	18.80×10^6	23.03×10^6
Total cost: greedy	5.62×10^6	10.30×10^6	14.82×10^6	19.31×10^6	23.71×10^6
$\sum_r$ Battery (kWh) : multiple	1223.6	1128.7	1082.9	1061.6	1052.0
$\sum_r$ Battery (kWh) : greedy	1314.4	1179.3	1142.6	1123.6	1108.1
Power track length (m) : multiple	5165	12715	21045	26130	29330
Power track length (m) : greedy	2955	8635	13060	16920	21110

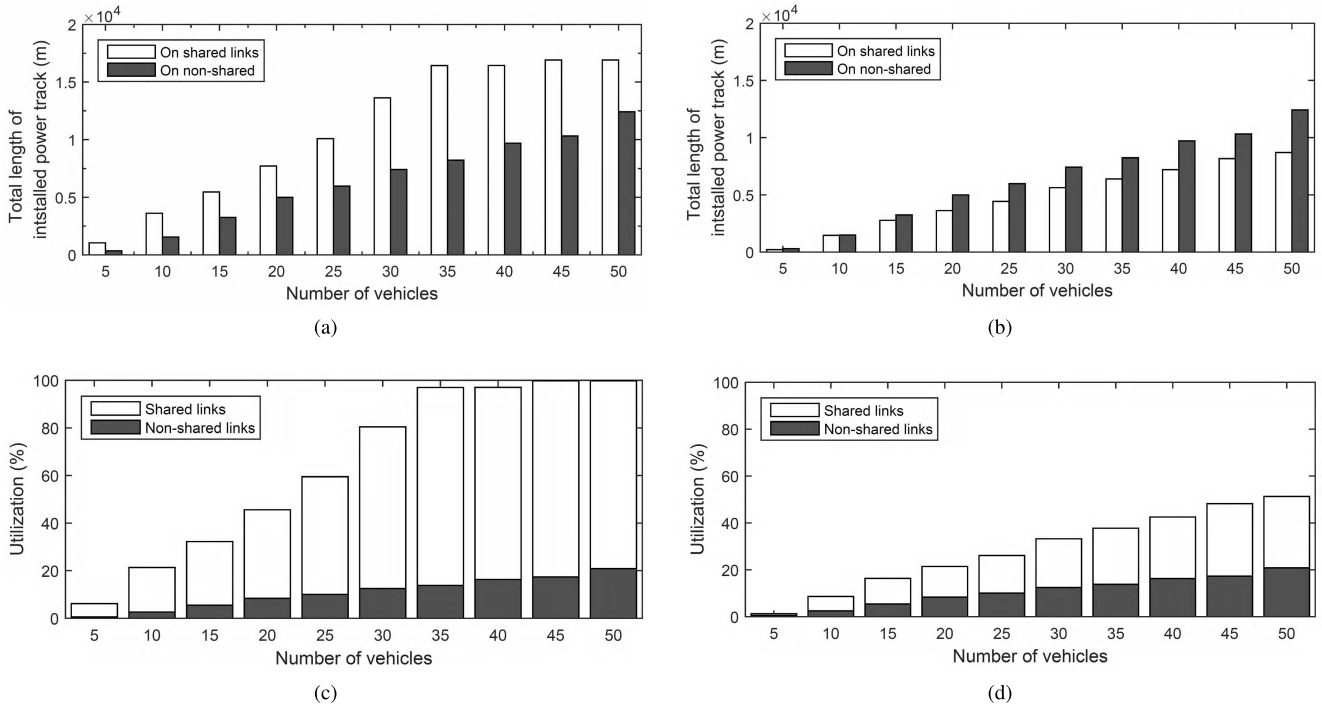

Fig. 13. Length of power track and utilization ratio of multiple route and greedy approach. (a) Total length of power tracks: Multiple route approach. (b) Total length of power tracks: Greedy approach. (c) Utilization ratio: Multiple route approach. (d) Utilization ratio: Greedy approach.

is a power source segment. Suppose the segments i to $i+5$ are selected as power source segments, then they compose a single power track 5 m in length. In this approach, each segment is a decision point – for example, if a segment is a power source, then 1, otherwise 0. The details of the model can be found in [29].

There are two drawbacks to the MIP-based model. First, it requires a significant number of decision variables. For instance, if the route is 30 km long and the segments are 1 m long, then 30,000 decision variables are needed. Jang et al. [29] showed that the MIP-based approach cannot be solved with commercial software such as IBM CPLEX for a practical problem. The other drawback of the MIP-based model is that due to its discrete nature, the solution depends on the level of resolution. Specifically, power track allocations may be radically different for 1 and 3 m segments. The discretized model with smaller segments may be more accurate, but it requires more computational power. Despite its significant limitations, we use the MIP approach to validate our model and algorithm due to their small scale.

The results from both the PSO and MIP approaches are presented in Table VII. We observed that the total cost obtained from the best result of the PSO algorithm was better than the result from MIP, as the former explores a continuous search space and the latter's solution quality is heavily dependent on the size of the unit segment. To obtain the same level of quality using MIP, we need to divide each segment into smaller pieces, but in this case, the running time of the exact solution algorithm becomes excessive.

D. Sensitivity Analysis

The goals of the sensitivity analysis presented in this subsection are to understand the model's system behavior and validate it with our insight. The system's key parameters–unit battery cost, fixed and variable power track costs–are independently varied, and we observe how the optimal allocation of power tracks and battery sizes is determined for each parameter setting.

Table VIII shows the parameters for the battery sensitivity analysis. The fixed and variable costs of the power tracks are unchanged while the battery cost varies from \$100 to \$1,000 in increments of \$100. Therefore, 10 different cases are generated and an optimal solution is evaluated for each case.

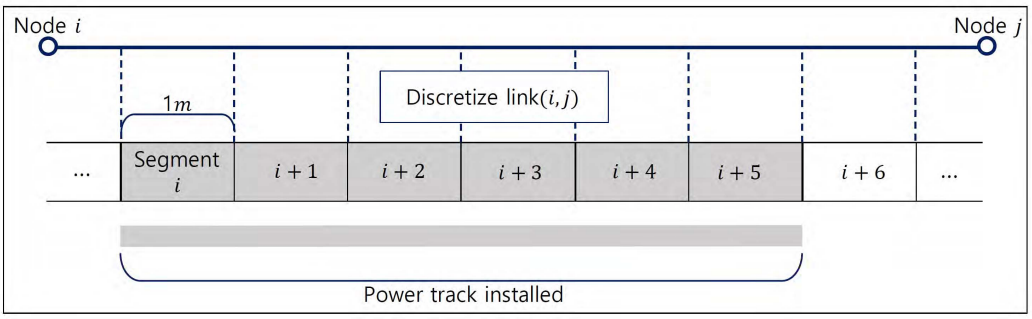

Fig. 14. Discretize link(i,j) into multiple segments 1 m long.

TABLE VII
OPTIMIZATION RESULTS FOR PSO ALGORITHM AND MIP

Description	PSO algorithm	MIP model
Total cost	7795928.12	7807481.63
Battery size Route 1	301.89 kWh	301.89 kWh
Battery size Route 2	123.15 kWh	123.21 kWh
Battery size Route 3	351.37 kWh	351.77 kWh
Battery size Route 4	280.04 kWh	280.09 kWh
Battery size Route 5	109.58 kWh	109.64 kWh
Total length of power track	8578.14 m	8715 m
Number of power tracks	57	57

TABLE VIII
PARAMETERS USED IN SENSITIVITY ANALYSIS - VARYING BATTERY COST

Parameter	Min	Max	Δ
Battery cost	\$100/kWh	\$1000/kWh	\$100/kWh
Fixed cost	\$5,000	\$5,000	-
Cable cost	\$60/m	\$60/m	-
# of vehicle	15	15	-

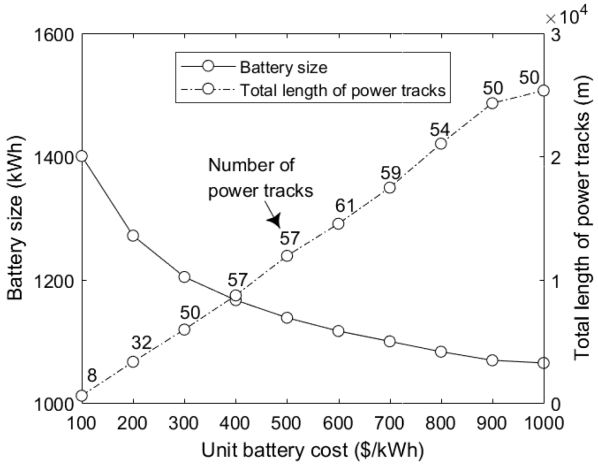

Fig. 15. Optimization results with varying unit battery costs.

TABLE IX
PARAMETERS USED IN SENSITIVITY ANALYSIS - FIXED COST OF POWER TRACKS

Parameter	Min	Max	Δ
Battery cost	\$400/kWh	\$400/kWh	-
Fixed cost	\$500	\$5,000	\$500
Cable cost	\$60/m	\$60/m	-
# of vehicle	15	15	-

Fig. 15 summarizes the results of the optimized cases. The x-axis indicates the varying battery cost from \$100 to \$1,000. The solid line that corresponds to the left side of the y-axis indicates the optimal battery sizes. The dashed line that corresponds to the right side of the y-axis indicates the optimized total length of the power tracks. The numbers along the line indicate the total number of power tracks installed on the routes.

The battery sensitivity analysis in Fig. 15 shows that when batteries are relatively cheap (\$100), a small number of power track installations is optimal; that is, the total length of the power track is around 570m (dashed line) and the number of power tracks is 8 (indicated above the line). Because the battery cost is low, it is cost-beneficial to equip the EVs with batteries large enough to sustain them across the entire multi-route system. As the battery cost increases, the optimal battery size tends to decrease. Instead, the total length of the power track increases. Evidently, it is more cost-effective to install additional charging areas and equip the vehicles with smaller batteries as the battery cost increases. Interestingly, when the battery cost is between \$600 and \$1,000, although the total length of the power track is monotonically increasing, the number of power tracks starts to decrease, from 61 to 50. We attribute this decrease to the sharing of routes in the multi-route system. Specifically, it might be beneficial to install fewer and longer power tracks if one of them is installed on a shared route. This behavior is not observed in single-route cases.

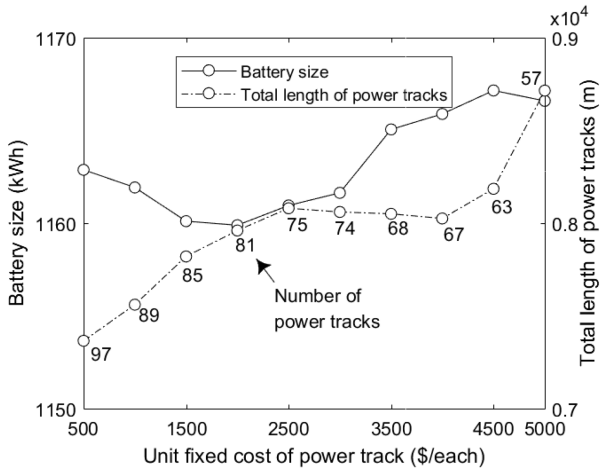

Fig. 16. Optimization results with varying unit fixed costs for the power tracks.

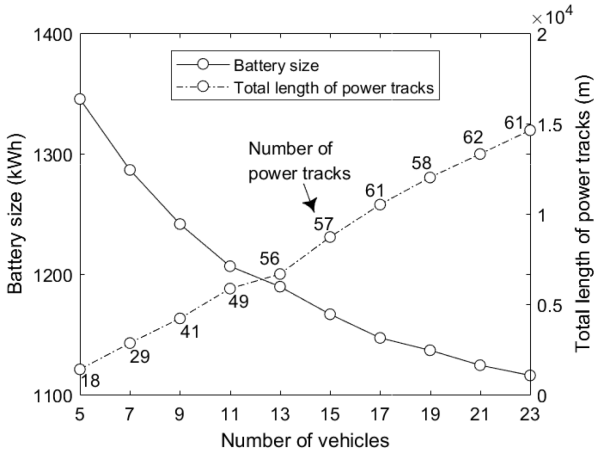

Fig. 17. Optimization results with varying number of vehicles on the route.

TABLE X
PARAMETERS USED IN SENSITIVITY ANALYSIS - TOTAL NUMBER OF VEHICLES

Parameter	Min	Max	Δ
Battery cost	$400/kWh	$400/kWh	-
Fixed cost	$5,000	$5,000	-
Cable cost	$60/m	$60/m	-
# of vehicle	5	23	2

The next case is the fixed-cost sensitivity analysis. The fixed cost of the power track varies while the rest of the cost parameters are fixed. The system parameters for the analysis are shown in Table IX. The results of the sensitivity analysis are summarized in Fig. 16.

The x-axis indicates the varying fixed costs of the power tracks from $500 to $5,000. The solid line to the left side of the y-axis indicates the optimal battery sizes. The dashed line to the right side of the y-axis indicates the optimized total length of the power tracks. The numbers along the dashed line indicate the total number of power tracks installed on the routes. In general, as the fixed cost of the power tracks increases, the optimal number of power tracks decreases; that is, the optimal number of tracks is 97 for $500, and 57 for $5,000. However, the total length of the power tracks does not exhibit a uniform trend. Depending on where the tracks are allocated, particularly whether they are located in the shared region of the route, the total length of the power track varies. This trend is somewhat different from the single-route case analyzed in [5], where an increase in the fixed cost of the power track always results in an increase in its total length, because it is cost-beneficial to have fewer power tracks with longer lengths rather than numerous short tracks. However, this intuitive behavior is not observed in the multi-route case.

Fig. 17 displays the results of the sensitivity analysis for the number of vehicles. The system parameters for the analysis are summarized in Table X.

The number of vehicles varies from 5 to 23. The solutions in the figure indicate that in general, the total length of the power tracks increases with the number of vehicles. The total battery cost decreases as more vehicles operate, making it cost-beneficial to invest more in the power tracks. However, although the total length increases, the number of power tracks fluctuates between around 50 and 60 depending on their allocation. Unlike in the single-route case, where both the total number and total length of the power tracks increase with the number of vehicles [5], these do not always increase together in the multi-route case.

The system behavior for the multi-route case indicates that the changes in the total length of the power tracks and battery size are similar to those found in the single-route case. In contrast, the behavior of the number of power tracks in the multi-route system does not always parallel that in the single-route case. The shared region on the route results in more complex power track allocation. These results show the complex nature of the problem, particularly for the multiple-route case. It is clearly difficult to allocate the power tracks without a rigorous, carefully designed model, such as that proposed in this work.

VI. CONCLUSION

In this paper, we provide a method for the optimization of DWC-EV transportation systems with key design variables; namely, power track allocation and battery size. Because the DWC-EV system uses road segments as charging facilities to supply electric energy to the vehicles, power track allocation decisions must consider the tracks' lengths and positions. Battery size decisions must also be considered in accordance with power track allocation. Therefore, our goal was to find an optimal DWC-EV system design that minimizes the total installation cost while maintaining the operational feasibility of EVs. We extended the previous research on single-route DWC-EV systems to address the multi-route systems common in urban public transportation. The issues that arose from this multi-route extension were discussed, and it was determined that the shared road segments must be treated as possible cost-beneficial candidates for installing power tracks.

We developed a mathematical model that optimally determines the design variables in a multi-route environment. Then, the PSO algorithm–a meta-heuristic approach–was proposed to solve the problem. We compared the performance of the PSO algorithm to the MIP model and concluded that the total cost of the system installation further improved with the PSO algorithm.

Using a numerical analysis, we generated meaningful findings on the problem. We proved that the multi-route optimization model provides superior results when compared with applying individual, single-route optimization to each route decomposed from the original multi-route environment. Because the model we developed captures the cost benefits of the shared road segments, it reduces the system's total construction cost by installing power tracks on these shared road segments. We also conducted a sensitivity analysis to determine the characteristics of the DWC-EV problem, and found that the solution changes with varying system parameters to clarify the DWC-EV system behavior.

The proposed modeling assumes a deterministic velocity profile. The actual velocity profile is not deterministic, and it would arguably be more realistic to model the velocity stochastically. However, because this study is one of the first attempts to model the multiple-route case, we decided to begin with the deterministic approach. We conceive this deterministic approach as a stepping stone to more complex modeling, including stochastic velocity models. This will be a productive topic for future research.

Nevertheless, this does not imply that the deterministic model described in this paper is less practical. The proposed optimization model can be run by engineers to determine the optimal locations and parameters of the power tracks. They can then run vehicle/traffic simulations with stochastic velocities to verify and validate the results from the optimization. The locations and parameters of the power tracks can be freely adjusted, based on the simulation results, to incorporate issues that had not been anticipated in the deterministic model. Formalizing this combined optimization and simulation approach represents another fruitful topic for future research.

Note that it is possible that two vehicles on different routes will arrive at a shared power track at the same time such that they both need to be charged simultaneously. In practice, we respond by letting one bus slow down if another bus is already on the power track. Although any operational issue is not a focus of this research, coordinating buses to avoid simultaneous charging on a power track can be solved by implementing appropriate operational rules such as regulating bus speeds and entrance times. The choice of an appropriate velocity trajectory and the associated operational problems are possible research topics. Another approach to this issue in the proposed optimization is to parameterize the fixed cost depending on the number of buses on the segment (i, j) such that $c_{fixed}(i, j) = F(k^r(i, j))$, or depending on the number of routes on the path segment $R(i, j)$ such that $c_{fixed}(i, j) = F(R(i, j))$. Thus, there are various possible solutions to this cost issue. Again, we leave the cost issue for future research.

APPENDIX
FIXED COST EVALUATION ALGORITHM

Details about the fixed cost evaluation algorithm introduced in section III are described in this appendix. Recall that Z is the binary indicator specifying which power track imposes the fixed cost. If $Z = 0$ for the corresponding power track, then it imposes the fixed cost and the other connected power tracks do not. The algorithm figures out the connectivity of the power tracks, and then specifies which imposes the fixed cost by evaluating the Z value for every power track.

The basic concept is as follows. First, the algorithm identifies whether power is located at the edge of the link. If the power track on the preceding link is located at the edge of the link, then it tries to identify whether there is any power track (succeeding power track) on other links connected through the intersection node. If there is a connected succeeding power track, we only impose the fixed cost at the succeeding, rather than the preceding, track. If there is more than one succeeding power track, we impose the fixed cost on the one with the highest link index number. In this case, only one unit of fixed cost is imposed for these connected power tracks. The details of the algorithm are explained in Figs. 18 and 19.

We first introduce the quantities used in the algorithm.

$$A^1_{(i,j)}(n') = \begin{cases} 1, & \text{if the power track } n' \text{ on } (i,j) \\ & \text{located at the end of } (i,j) \\ 0, & \text{otherwise} \end{cases}$$
$$= Max\left[0, \left\lceil \epsilon \left\{x^e_{(i,j)}(n') - x^s_{(i,j)}(n')\right\} \cdot \times \left\{x^e_{(i,j)}(n') - l_{(i,j)} + \epsilon\right\} \right\rceil\right], \quad (18)$$

$$B^1_{(i,j)}(n') = \begin{cases} 1, & \text{if a power track exists at the} \\ & \text{beginning of the succeeding} \\ & \text{power track } (j,k) \in \mathbf{L} \\ 0, & \text{otherwise} \end{cases}$$
$$= Max\left[0, \left\lceil \epsilon \sum_{\forall_c} \left\{x^e_{(j,k)}(1) - x^s_{(j,k)}(1)\right\} \cdot \times \left\{0 - x^s_{(j,k)}(1) + \epsilon\right\} \right\rceil\right], \quad (19)$$

where $0 < \epsilon \ll 1$. The quantity $A^1_{(i,j)}(n')$ identifies the position of $PT_{(i,j)}(n')$ as shown in Fig.18(a). The quantity $B^1_{(i,j)}(n')$ identifies whether $PT_{(i,j)}(n')$ has any connected power tracks in the succeeding links, as shown in 18(b).

With the quantities A and B, Z identifies whether $PT(n')$ is a power track followed by another power track in a succeeding link with the following equation:

$$Z^1_{(i,j)}(n') = A^1_{(i,j)}(n')B^1_{(i,j)}(n') \quad (20)$$

As this figure shows, the $PT_{(i,j)}(n')$ in Fig.18(e) is located at the end of its link $(A = 1)$ and connected to two more power tracks in the succeeding links $(B = 1)$, therefore, $Z = 1$. Because the algorithm only imposes the fixed cost

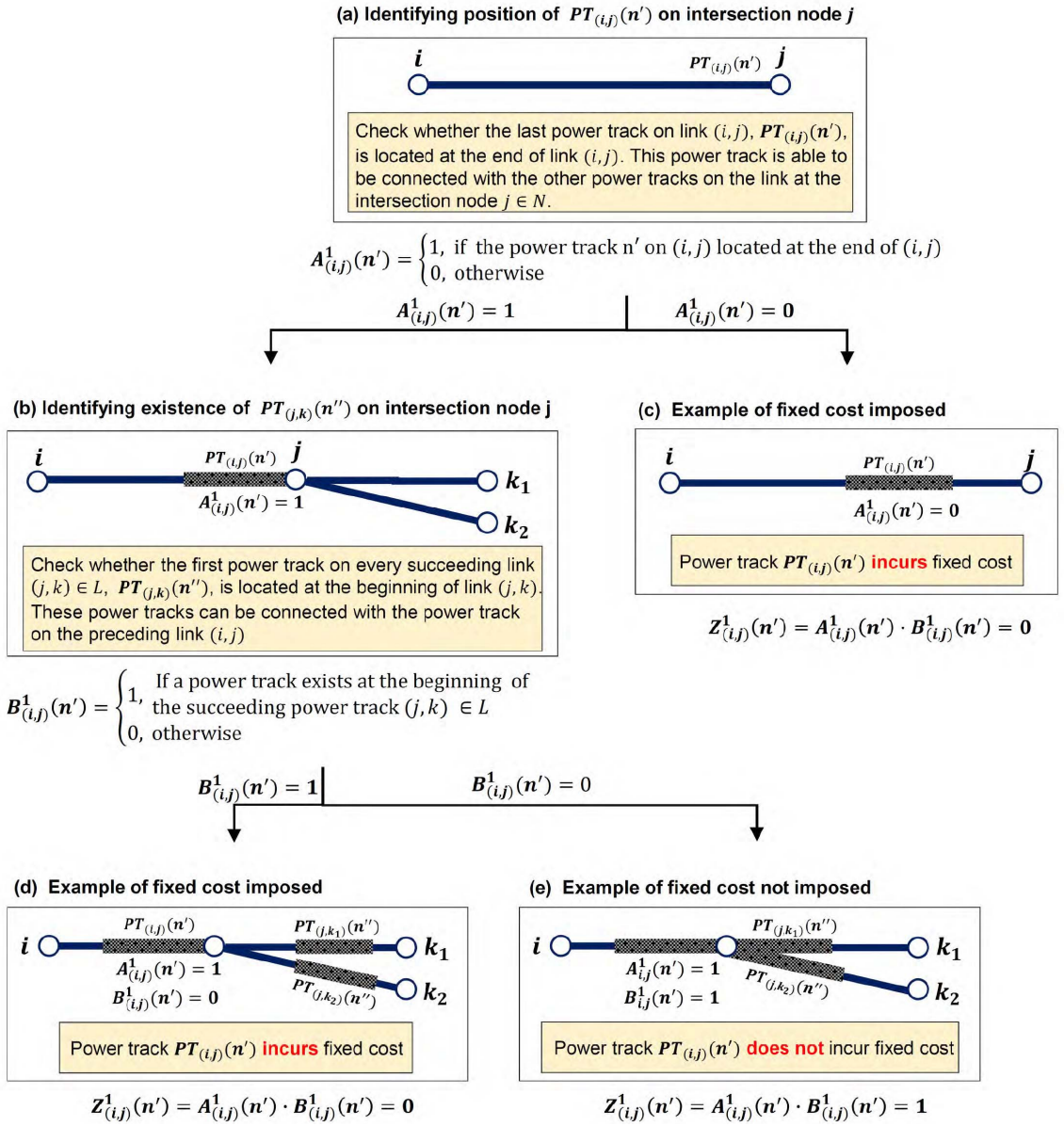

Fig. 18. Fixed cost counting algorithm: Power track on preceding link.

on the last power track on the link with the highest index number, the $PT_{(i,j)}(n')$ is not imposed on the fixed cost. Let us consider the power tracks $PT_{(j,k_1)}(n'')$ and $PT_{(j,k_2)}(n'')$ in Fig.19. In this case, the algorithm's point of interest is moved to the power tracks connected by a preceding power track. For our convenience, we define the following quantities:

$$A^2_{(j,k)}(n'') = \begin{cases} 1, & \text{if the power track } n'' \text{ on } (j,k) \text{ is located at the beginning of } (j,k) \\ 0, & \text{otherwise} \end{cases}$$
$$= Max\left[0, \left\lceil \epsilon \left\{x^e_{(i,j)}(n'') - x^s_{(i,j)}(n'')\right\} \cdot \times \left\{0 - x^s_{a,b}(i) + \epsilon\right\} \right\rceil\right], \quad (21)$$

$$B^2_{(j,k)}(n'') = \begin{cases} 1, & \text{, if there is a power track at the beginning of the link } (j,k') \\ & \text{where } k' > k \text{ at intersection } j \\ 0, & \text{otherwise} \end{cases}$$
$$= Max\left[0, \left\lceil \epsilon \sum_{\forall k' | k' > k} \left\{x^e_{(j,k')}(1) - x^s_{(j,k')}(1)\right\} \cdot \times \left\{0 - x^s_{j,k'}(1) + \epsilon\right\} \right\rceil\right], \quad (22)$$

where $0 < \epsilon \ll 1$. In Fig.19, $PT_{(j,k_1)}(n'')$ is located at the beginning of link (j,k_1), so $A^2_{(j,k_1)}(n'')$ is 1. According to the definition of B^2, if there is no power track like the one $PT_{(j,k_1)}(n'')$ in link (j,k_2), where $k_2 > k_1$, then B^2 is 0. If there are multiple power tracks located at node j and the one in link (j,k_2) exists, then B^2 $is1$. For example, in Fig.19(c),

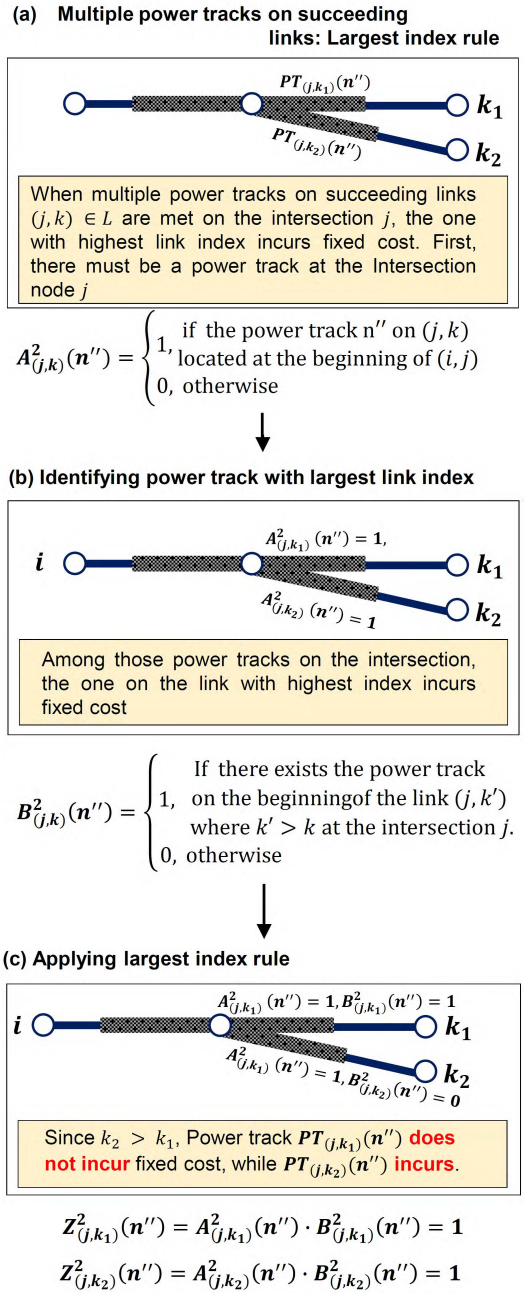

Fig. 19. Fixed cost counting algorithm: Power track on succeeding link.

both $PT_{(j,k_1)}(n'')$ and $PT_{(j,k_2)}(n'')$ start from node j, but $PT_{(j,k_2)}(n'')$ has a higher index number than $PT_{(j,k_1)}(n'')$, and therefore, $B^2_{(j,k_2)}(n'')$ is 0 and $B^2_{(j,k_1)}(n'')$ is 1.

$$Z^2_{(j,k_1)}(n'') = A^2_{(j,k_1)}(n'')B^2_{(j,k_1)}(n'') = 1 \quad (23)$$

$$Z^2_{(j,k_2)}(n'') = A^2_{(j,k_2)}(n'')B^2_{(j,k_2)}(n'') = 0 \quad (24)$$

With the quantities Z^1 and Z^2, we determined whether the power track under consideration carried the fixed cost. For example, In Fig.19(c), $PT_{(j,k_2)}(n'')$ is imposed fixed cost.

REFERENCES

[1] Y. J. Jang, E. S. Suh, and J. W. Kim, "System architecture and mathematical models of electric transit bus system utilizing wireless power transfer technology," *IEEE Syst. J.*, vol. 10, no. 2, pp. 495–506, Jun. 2016.

[2] S. Lukic and Z. Pantic, "Cutting the cord: Static and dynamic inductive wireless charging of electric vehicles," *IEEE Electrific. Mag.*, vol. 1, no. 1, pp. 57–64, Sep. 2013.

[3] S. Ahn, N. P. Suh, and D.-H. Cho, "Charging up the road," *IEEE Spectr.*, vol. 50, no. 4, pp. 48–54, Apr. 2013.

[4] L. Kelion. (2013). *South Korean Road Wirelessly Recharges OLEV Buses*. [Online]. Available: http://www.bbc.com/news/technology-23603751

[5] Y. D. Ko and Y. J. Jang, "The optimal system design of the online electric vehicle utilizing wireless power transmission technology," *IEEE Trans. Intell. Transp. Syst.*, vol. 14, no. 3, pp. 1255–1265, Sep. 2013.

[6] J. G. Bolger, F. A. Kirsten, and L. S. Ng, "Inductive power coupling for an electric highway system," in *Proc. 28th IEEE Veh. Technol. Conf.*, vol. 28. Mar. 1978, pp. 137–144.

[7] A. Esser, "Contactless charging and communication for electric vehicles," *IEEE Ind. Appl. Mag.*, vol. 1, no. 6, pp. 4–11, Nov. 1995.

[8] D. A. G. Pedder, A. D. Brown, and J. A. Skinner, "A contactless electrical energy transmission system," *IEEE Trans. Ind. Electron.*, vol. 46, no. 1, pp. 23–30, Feb. 1999.

[9] H. Ayano, K. Yamamoto, N. Hino, and I. Yamato, "Highly efficient contactless electrical energy transmission system," in *Proc. IEEE 28th Annu. Conf. Ind. Electron. Soc.*, vol. 2. Nov. 2002, pp. 1364–1369.

[10] H. H. Wu, J. T. Boys, and G. A. Covic, "An AC processing pickup for IPT systems," *IEEE Trans. Power Electron.*, vol. 25, no. 5, pp. 1275–1284, May 2010.

[11] C.-Y. Huang, J. T. Boys, G. A. Covic, and M. Budhia, "Practical considerations for designing IPT system for EV battery charging," in *Proc. IEEE Veh. Power Propuls. Conf.*, Sep. 2009, pp. 402–407.

[12] M. Budhia, G. A. Covic, and J. T. Boys, "Design and optimization of circular magnetic structures for lumped inductive power transfer systems," *IEEE Trans. Power Electron.*, vol. 26, no. 11, pp. 3096–3108, Nov. 2011.

[13] N. P. Suh, D. H. Cho, and C. T. Rim, *Design of On-Line Electric Vehicle (OLEV)*. Berlin, Germany: Springer, 2011, pp. 3–8.

[14] J. Huh, S. Lee, C. Park, G.-H. Cho, and C.-T. Rim, "High performance inductive power transfer system with narrow rail width for on-line electric vehicles," in *Proc. IEEE Energy Convers. Congr. Expo.*, Sep. 2010, pp. 647–651.

[15] S. Ahn *et al.*, "Low frequency electromagnetic field reduction techniques for the on-line electric vehicle (OLEV)," in *Proc. IEEE Int. Symp. Electromagn. Compat. (EMC)*, Jul. 2010, pp. 625–630.

[16] S. Ahn and J. Kim, "Magnetic field design for high efficient and low EMF wireless power transfer in on-line electric vehicle," in *Proc. 5th Eur. Conf. Antennas Propag. (EUCAP)*, Apr. 2011, pp. 3979–3982.

[17] J. Shin *et al.*, "Design and implementation of shaped magnetic-resonance-based wireless power transfer system for roadway-powered moving electric vehicles," *IEEE Trans. Ind. Electron.*, vol. 61, no. 3, pp. 1179–1192, Mar. 2014.

[18] N. P. Suh and D. H. Cho, *The On-Line Electric Vehicle: Wireless Electric Ground Transportation Systems*. Springer, 2017.

[19] A. Ip, S. Fong, and E. Liu, "Optimization for allocating BEV recharging stations in urban areas by using hierarchical clustering," in *Proc. 6th Int. Conf. Adv. Inf. Manage. Service (IMS)*, Nov./Dec. 2010, pp. 460–465.

[20] S. Ge, L. Feng, and H. Liu, "The planning of electric vehicle charging station based on grid partition method," in *Proc. Int. Conf. Elect. Control Eng. (ICECE)*, Sep. 2011, pp. 2726–2730.

[21] S. MirHassani and R. Ebrazi, "A flexible reformulation of the refueling station location problem," *Transp. Sci.*, vol. 47, no. 4, pp. 617–628, 2012.

[22] M. Kuby and S. Lim, "The flow-refueling location problem for alternative-fuel vehicles," *Soc.-Econ. Planning Sci.*, vol. 39, no. 2, pp. 125–145, 2005.

[23] M. Wen, G. Laporte, O. B. G. Madsen, A. V. Nørrelund, and A. Olsen, "Locating replenishment stations for electric vehicles: Application to Danish traffic data," *J. Oper. Res. Soc.*, vol. 65, no. 10, pp. 1555–1561, 2013.

[24] P.-S. You and Y.-C. Hsieh, "A hybrid heuristic approach to the problem of the location of vehicle charging stations," *Comput. Ind. Eng.*, vol. 70, pp. 195–204, Apr. 2014.

[25] M. Yilmaz and P. T. Krein, "Review of the impact of vehicle-to-grid technologies on distribution systems and utility interfaces," *IEEE Trans. Power Electron.*, vol. 28, no. 12, pp. 5673–5689, Dec. 2013.

[26] Z. Pantic, S. Bai, and S. M. Lukic, "Inductively coupled power transfer for continuously powered electric vehicles," in *Proc. IEEE Veh. Power Propuls. Conf.*, Sep. 2009, pp. 1271–1278.

[27] Z. Chen, F. He, and Y. Yin, "Optimal deployment of charging lanes for electric vehicles in transportation networks," *Transp. Res. B, Methodol.*, vol. 91, pp. 344–365, Sep. 2016.
[28] Z. Chen, W. Liu, and Y. Yin, "Deployment of stationary and dynamic charging infrastructure for electric vehicles along traffic corridors," *Transp. Res. C, Emerg. Technol.*, vol. 77, pp. 185–206, Apr. 2017.
[29] Y. J. Jang, S. Jeong, and Y. D. Ko, "System optimization of the on-line electric vehicle operating in a closed environment," *Comput. Ind. Eng.*, vol. 80, pp. 222–235, Feb. 2015.
[30] J. Wang, C. Liu, D. Ton, Y. Zhou, J. Kim, and A. Vyas, "Impact of plug-in hybrid electric vehicles on power systems with demand response and wind power," *Energy Policy*, vol. 39, no. 7, pp. 4016–4021, 2011.
[31] F. He, D. Wu, Y. Yin, and Y. Guan, "Optimal deployment of public charging stations for plug-in hybrid electric vehicles," *Transp. Res. B, Methodol.*, vol. 47, pp. 87–101, Jan. 2013.
[32] A. Ashtari, E. Bibeau, S. Shahidinejad, and T. Molinski, "PEV charging profile prediction and analysis based on vehicle usage data," *IEEE Trans. Smart Grid*, vol. 3, no. 1, pp. 341–350, Mar. 2012.
[33] S. Mohrehkesh and T. Nadeem, "Toward a wireless charging for battery electric vehicles at traffic intersections," in *Proc. 14th Int. IEEE Conf. Intell. Transp. Syst. (ITSC)*, Oct. 2011, pp. 113–118.
[34] J. Kennedy and R. Eberhart, "Particle swarm optimization," in *Proc. IEEE Int. Conf. Neural Netw.*, vol. 4. Nov. 1995, pp. 1942–1948.
[35] Y. Shi and R. Eberhart, "A modified particle swarm optimizer," in *Proc. IEEE World Congr. Comput. Intell. Evol. Comput.*, May 1998, pp. 69–73.
[36] Y. Shi and R. C. Eberhart, "Empirical study of particle swarm optimization," in *Proc. Congr. Evol. Comput. (CEC)*, vol. 3. Jul. 1999, pp. 1945–1950.
[37] D. W. Boeringer and D. H. Werner, "Particle swarm optimization versus genetic algorithms for phased array synthesis," *IEEE Trans. Antennas Propag.*, vol. 52, no. 3, pp. 771–779, Mar. 2004.
[38] S. He, Q. H. Wu, J. Y. Wen, J. R. Saunders, and R. C. Paton, "A particle swarm optimizer with passive congregation," *Biosystems*, vol. 78, nos. 1–3, pp. 135–147, 2004.
[39] Y. Shi and R. C. Eberhart, "Parameter selection in particle swarm optimization," in *Evolutionary Programming VII*. Berlin, Germany: Springer, Dec. 2005, pp. 591–600.
[40] J.-G. Kim and M. Kuby, "The deviation-flow refueling location model for optimizing a network of refueling stations," *Int. J. Hydrogen Energy*, vol. 37, no. 6, pp. 5406–5420, 2012.
[41] F. Jiménez, S. Tapia-Fernández, and W. Cabrera-Montiel, "System for road vehicle energy optimization using real time road and traffic information," *Energies*, vol. 7, no. 6, pp. 3576–3598, 2014.

Illhoe Hwang received the B.S. degree and the M.S. degree in industrial engineering from the Korea Advanced Institute of Science and Technology, Daejeon, South Korea, in 2014, where he is currently pursuing the Ph.D. degree. His research interests include the mathematical modeling of complex systems, system optimizations, simulation and logistics systems.

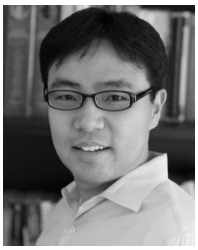

Young Jae Jang received the B.S. degree in aerospace engineering from Boston University in 1997, and the double M.S. degree in mechanical engineering and operations research and the Ph.D. degree in mechanical engineering from the Massachusetts Institute of Technology in 2001 and 2007, respectively. He is currently an Assistant Professor with the Department of Industrial and Systems Engineering, Korea Advanced Institute of Science and Technology (KAIST). He is also affiliated with the Cho Chun Shik Graduate School of Green Transportation, KAIST. His current research includes the stochastic modeling of complex systems and optimizations in transportation and logistics systems. He has been involved in the KAIST On-Line Electric Vehicle project developing and commercializing the innovative wireless charging electric vehicle. The project was recognized as the 50 Best Innovations of 2010 by *TIME Magazine*. His role in the project is to develop the optimal energy management system to integrate the vehicle system to the road traffic network. He has authored or co-authored numerous technical papers out of the OLEV technology. His recent work The Optimal Economic Design of the Wireless Powered Transportation System was selected as the Best Paper at the 2013 International Conference on Intelligent Manufacturing and Logistics Conference. He was the Technical Program Chair of the 2014 IEEE Vehicular Technology Workshop on Emerging Technologies on Wireless Power and the Organizing Committee Member of the Complex Systems Design & Management Asia 2014. Before he joined KAIST, he was with Micron Technology, Inc., VA, USA, as a Project Manager, he led a global initiative to improve the efficiency of the manufacturing facilities located worldwide. While working at Micron, he was also involved in activities supporting the company's operational and strategic decision making using quantitative modeling and analysis techniques.

Young Dae Ko received the B.S. degree in industrial engineering and the Ph.D. degree in industrial and systems engineering from the Korea Advanced Institute of Science and Technology (KAIST) in 2004 and 2011, respectively. He was a Post-Doctoral Researcher with the Industrial Engineering and Management Research Institute, KAIST, from 2011 to 2013. He was with the Data Analytics Group of Deloitte Consulting as a Manager from 2013 to 2016. He has performed numerous industry projects concerning big data and business analytics. He is currently an Assistant Professor with the Department of Hotel and Tourism Management, Sejong University, Seoul, South Korea. His research interests include business analytics, revenue management, system optimization, and green transportation.

Min Seok Lee received the B.S. degree and the M.S. degree in industrial engineering from the Korea Advanced Institute of Science and Technology, Daejeon, South Korea, in 2014 and 2016, respectively, where he is currently pursuing the Ph.D. degree. His research interests include system optimizations, modeling and design of transportation systems and logistics systems.